Cell PRESS
Open ACCESS

Cell Reports
Report

A Genetic Screen Identifies TCF3/E2A and TRIAP1 as Pathway-Specific Regulators of the Cellular Response to p53 Activation

Zdenek Andrysik,[1] Jihye Kim,[2] Aik Choon Tan,[2] and Joaquín M. Espinosa[1,*]
[1]Howard Hughes Medical Institute & Department of Molecular, Cellular and Developmental Biology, University of Colorado at Boulder, Boulder, CO 80309, USA
[2]Department of Medicine/Medical Oncology, University of Colorado at Denver Anschutz Medical Campus, Aurora, CO 80045, USA
*Correspondence: joaquin.espinosa@colorado.edu
http://dx.doi.org/10.1016/j.celrep.2013.04.014

SUMMARY

The p53 transcription factor participates in diverse cellular responses to stress, including cell-cycle arrest, apoptosis, senescence, and autophagy. The molecular mechanisms defining the ultimate outcome of p53 activation remain poorly characterized. We performed a genome-wide genetic screen in human cells to identify pathway-specific coregulators of the p53 target gene *CDKN1A* (p21), an inhibitor of cell-cycle progression, versus *BBC3* (PUMA), a key mediator of apoptosis. Our screen identified numerous factors whose depletion creates an imbalance in the p21:PUMA ratio upon p53 activation. The transcription factor TCF3, also known as E2A, drives p21 expression while repressing PUMA across cancer cell types of multiple origins. Accordingly, TCF3/E2A depletion impairs the cell-cycle-arrest response and promotes apoptosis upon p53 activation by chemotherapeutic agents. In contrast, TRIAP1 is a specific repressor of p21 whose depletion slows down cell-cycle progression. Our results reveal strategies for driving cells toward specific p53-dependent responses.

INTRODUCTION

The p53 transcription factor functions as a signaling hub during the cellular response to stress. p53 is activated by various signaling cascades elicited by myriad stress stimuli, including oncogene hyperactivation, DNA damage, and nutrient deprivation (Vousden and Prives, 2009). These signaling pathways relieve the inhibitory effects of the p53 repressors MDM2 and MDM4, which otherwise target p53 for proteasomal degradation and mask its transactivation domain. Upon activation, p53 induces transcription of genes involved in varied cellular responses such as cell-cycle arrest, apoptosis, senescence, and autophagy (Riley et al., 2008). Although many p53 target genes participating in each pathway have been identified, the mechanisms defining which cellular response is adopted remain poorly characterized. A thorough understanding of these mechanisms of cell-fate choice will be required for the effective deployment of p53-based therapies in the clinic. Currently, small molecule inhibitors of MDM2 and MDM4 are being tested in clinical trials for cancer treatment (Brown et al., 2009). However, the cellular response elicited by these compounds varies greatly across cancer cell types (París et al., 2008; Sullivan et al., 2012b; Tovar et al., 2006). Thus, the identification of factors that regulate cell-fate choice upon p53 activation would reveal strategies to enhance the therapeutic application of these drugs.

Many efforts in the p53 field have been devoted to the characterization of p53 posttranslational modifications and p53 cofactors as well as p53-autonomous mechanisms driving gene-specific regulation within the p53 transcriptional program (Vousden and Prives, 2009). With the advent of functional genomics, it is now possible to perform genetic screens in human cells for the unbiased identification of pathway-specific coregulators of p53 target genes. We report here the results of a genome-wide short hairpin RNA (shRNA) genetic screen to identify factors that regulate the expression ratio between *CDKN1A* (p21), one of the key mediators of p53-dependent cell-cycle arrest, and *BBC3* (PUMA), a BH3-only protein that mediates much of the apoptotic effects of p53. Using a flow cytometry assay to isolate cells with altered expression of the endogenous p21 and PUMA proteins and a DNA deep-sequencing protocol to identify the shRNAs expressed in these cells, we found numerous factors that affect the p21:PUMA ratio. Most prominent among these was TCF3 (transcription factor 3, also known as E2A), a basic helix-loop-helix (bHLH) DNA binding protein that is required for p21 induction, yet functions as a repressor of PUMA. Depletion of TCF3/E2A leads to lower p21 accumulation and higher PUMA expression across cancer cell types of diverse tissue origin, thus promoting the apoptotic response upon p53 activation. Additionally, we identified TRIAP1 (TP53-regulated inhibitor of apoptosis, also known as p53 cell survival factor or p53CSV) as a gene-specific repressor of p21. TRIAP1 knockdown leads to augmented p21 expression before and during p53 activation and slows down cell proliferation. Overall, our research identified multiple factors that function as gene-specific coregulators within the p53 network and reveals several strategies to manipulate the cellular response upon p53 activation.

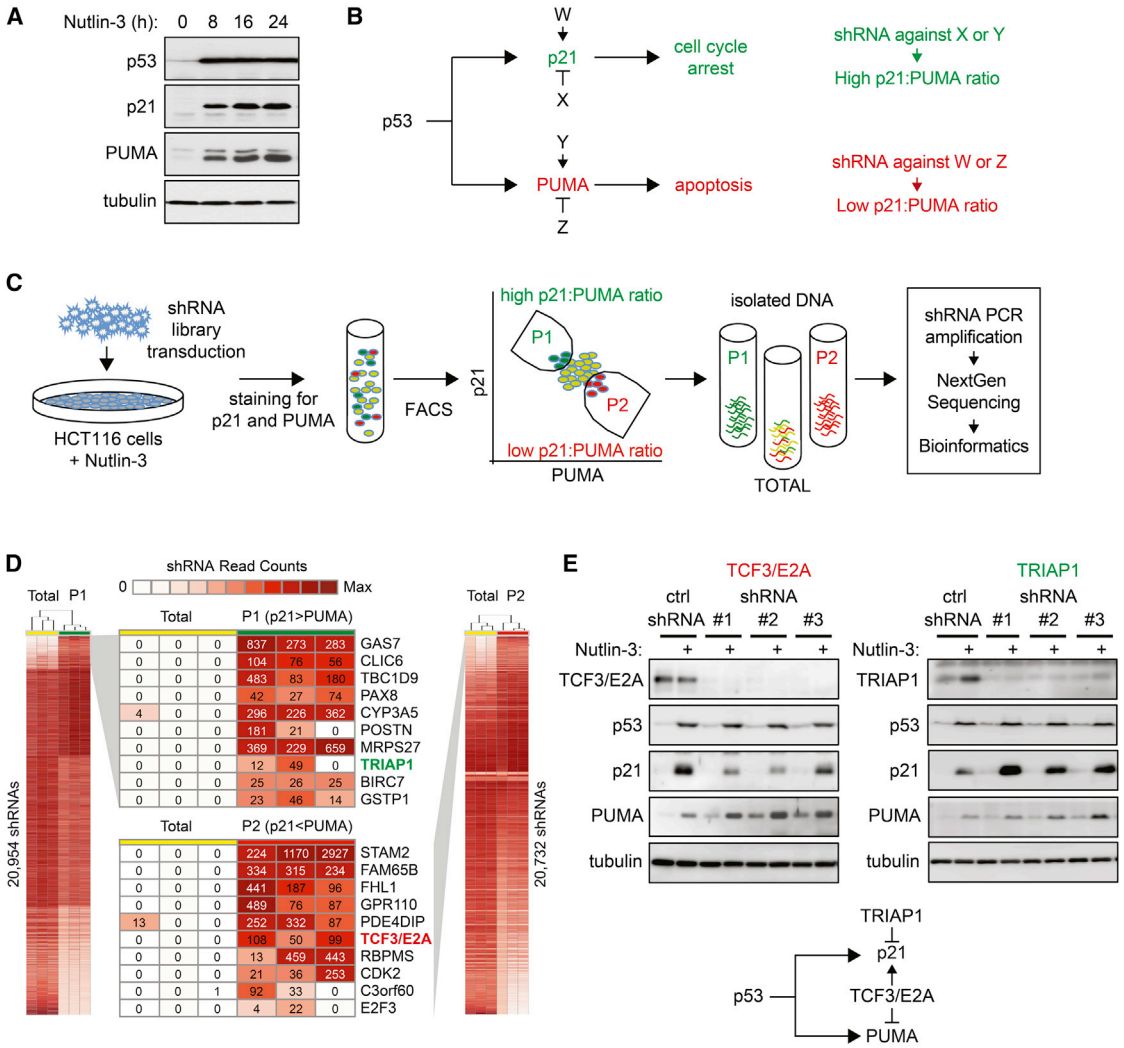

Figure 1. A Genome-wide shRNA Screen Identifies Pathway-Specific Regulators within the p53 Network

(A) Western blot assays showing that activation of p53 with Nutlin-3 leads to concurrent induction of p21 and PUMA in HCT116 cells.

(B) Hypothetical factors W, X, Y, and Z function as gene-specific coregulators of p21 and PUMA.

(C) Experimental design for shRNA screen leading to identification of gene-specific coregulators of p21 and PUMA.

(D) Heatmaps showing differential counts of shRNAs in the sorted populations dubbed P1 (high p21:PUMA ratio) and P2 (low p21:PUMA ratio) versus the total population. Numbers represent the shRNA count in the three sets of triplicates.

(E) Different shRNAs against TCF3/E2A and TRIAP1 change the p21:PUMA expression ratio as predicted by the genetic screen. TCF3/E2A depletion reduces p21 expression and increases PUMA expression without affecting p53 accumulation. TRIAP1 knockdown leads to increased p21 expression with no effects on PUMA or p53 accumulation.

See also Figure S1.

RESULTS

A Genetic Screen in Human Cells for the Identification of Factors Regulating the p21:PUMA Expression Ratio upon p53 Activation

p53 activation commonly leads to concurrent induction of target genes in distinct functional pathways, yet the precise cellular response adopted varies widely across cell types. In HCT116 colorectal cancer cells, p53 activation with Nutlin-3, a small molecule inhibitor of the p53-MDM2 interaction, leads to strong induction of both p21 and PUMA (Figure 1A). In this scenario, HCT116 cells undergo cell-cycle arrest, but become highly sensitized to additional apoptotic stimuli (Henry et al., 2012; Sullivan et al., 2012b). We hypothesized the existence of pathway-specific coregulators with the ability to control the p21:PUMA expression ratio in this setting and thus affect the cell-fate choice upon p53 activation (factors W, X, Y, and Z in Figure 1B). These coregulators would function as gene-specific coactivators or repressors of p21 or PUMA. According to this hypothesis, whereas an shRNA against factors X or Y would lead to a greater p21:PUMA expression ratio, an shRNA against factors W or Z would decrease this ratio (Figure 1B). In order to identify these factors, we designed

a genome-wide shRNA screen as depicted in Figure 1C. First, we transduced a lentiviral shRNA library targeting >16,000 human genes (SBI library) into HCT116 cells. After antibiotic selection of stable integrants and clearance of cells carrying shRNAs against essential genes during 2 weeks of culture, we activated p53 with Nutlin-3 and isolated cells expressing different ratios of endogenous p21 and PUMA by fluorescence activated cell sorting (FACS). After intensive testing of multiple fixation/staining conditions and antibodies, we obtained a protocol that robustly detects a p53-dependent increase in the levels of the endogenous p21 and PUMA proteins by flow cytometry (Figures S1A and S1B; see the Extended Experimental Procedures), which enabled us to sort cells with varying p21:PUMA ratios during the screen. Whereas the population dubbed P1 stained strongly for p21 and weakly for PUMA, the P2 population stained strongly for PUMA and weakly for p21. We then isolated DNA from P1, P2, and the input population (total) and amplified shRNAs by PCR with primers against the flanking sequences. In a nested PCR, we tagged the shRNA cassettes for Illumina deep sequencing and sequenced three biological replicates of each population. Using a bioinformatics pipeline dubbed BiNGS (*Bi*oinformatics for *N*ext *G*eneration *S*equencing) (Kim and Tan, 2012), we identified shRNAs whose abundance was significantly different between P1 versus total and P2 versus total (Figure 1D). Of note, we found many shRNAs that fell below the level of detection in the total population yet could be counted hundreds of times in either P1 or P2. Importantly, BiNGS takes into account how many shRNAs against a given messenger RNA (mRNA) display the same behavior, a concept dubbed "reagent redundancy" in RNA interference (RNAi) screens, which reduces the chances of false positives due to "off-target" effects of individual shRNAs (Echeverri et al., 2006). The information on shRNA multiplicity is then condensed into a *p(wZ)* value for each gene (Figure S1C) (see the Extended Experimental Procedures for details). Using a cutoff of $p(wZ) < 0.01$, we identified 491 candidate genes whose knockdown would create an increase in the p21:PUMA ratio and 523 candidate genes exerting the opposite effect (Figure S1C; Table S1). Next, we selected ~40 candidate genes in each category for validation and established stable knockdowns in HCT116 cells for each of them (see the Extended Experimental Procedures for selection criteria; Table S2). Importantly, during these validation efforts we utilized shRNAs from a different library (TRC, The RNAi Consortium). Since the seed sequences in the TRC shRNAs are different from those in the SBI shRNAs used in the initial screen, this exercise significantly increased our confidence in positively validated results. In order to test the effect of the 81 individual knockdowns on the p21:PUMA ratio, we employed a dual-fluorescence western blot assay that enabled us to monitor p21 and PUMA protein expression within the same blot (see example in Figure S1D). Because this assay bypasses the fixation steps involved in the flow cytometry assay used for the screen, which could potentially create artifacts, it increased the stringency of our validation efforts. When using a cutoff of 20% change in the p21:PUMA protein ratio relative to a nontargeting shRNA control, this assay led to the identification of 12 genes whose knockdown tips the balance toward more PUMA (e.g., *TCF3/E2A*, *C3orf60*, *GPR110*) and seven genes with the opposite effect (e.g., *TRIAP1*, *GSPT1*, *POSTN*) (Figures 1E and S1E; Table S2).

From these validation efforts, we selected two factors for further study, TCF3/E2A and TRIAP1, whose depletion produced the most pronounced changes in p21:PUMA expression. Knockdown of TCF3/E2A with three different shRNAs leads to decreased p21 induction and increased PUMA expression upon Nutlin-3 treatment, without affecting p53 accumulation (Figure 1E). In contrast, depletion of TRIAP1 with three different shRNAs leads to stronger p21 induction with negligible effects on PUMA expression or p53 accumulation. Thus, TCF3/E2A works concurrently as a coactivator of p21 and repressor of PUMA, while TRIAP1 behaves as a gene-specific repressor of p21 (Figure 1E, diagram).

Taken together, these results demonstrate that our genetic screen successfully identified regulators of the p21:PUMA expression ratio, which could potentially modulate the cellular response to p53 activation.

TCF3/E2A and TRIAP1 Are Conserved Specific Coregulators of the p21:PUMA Expression Ratio

The cellular response to p53 activation varies greatly across cell types. Several gene-specific regulators of p53 target genes have been identified, but their action is often restricted to specific cell types (Sullivan et al., 2012a; Vousden and Prives, 2009). In order to test for the conservation of TCF3/E2A and TRIAP1 effects, we defined their impact across three cancer cell types of diverse tissue origins during a time course of Nutlin-3 treatment between 6 and 48 hr. Importantly, TCF3/E2A knockdown leads to decreased p21 induction and increased PUMA expression in HCT116 cells (colorectal carcinoma), U2OS cells (osteosarcoma), and A549 cells (lung carcinoma) at multiple time points (Figures 2A and S2A). Of note, TCF3/E2A depletion had no significant effects on the extent and kinetics of p53 accumulation, suggesting that this factor acts downstream or in parallel to p53. Interestingly, TCF3/E2A expression decreases upon Nutlin-3 treatment in all three cell types tested, but not in HCT116 $p53^{-/-}$ cells (Figures 2A, S2A, and S2C). Of note, TCF3/E2A levels are also downregulated over prolonged time in cell culture regardless of p53 status, which correlates with decreased proliferation rates (Figures S2C and S2D), and this downregulation is also observed at the mRNA level (Figures S2E and S2F). Overall, these results indicate that TCF3/E2A expression is higher in proliferating cells and downregulated by p53-dependent and -independent cell-cycle arrest. Next, we investigated the effect of TCF3/E2A depletion on expression of the p21 and PUMA mRNAs using quantitative RT-PCR. In fact, TCF3/E2A knockdown decreases p21 mRNA accumulation while enhancing PUMA mRNA induction at multiple time points in every cell line tested (Figure 2A and S2A). Of note, TCF3/E2A knockdown also affects the basal expression levels of p21 mRNA (see Figure S2G for replotting of the basal expression data at a lower scale). Interestingly, TCF3/E2A does not affect the induced expression of several additional p53 target genes in various functional pathways, thus demonstrating its highly specific effects toward p21 and PUMA in this setting (Figure 2C). Altogether, our results demonstrate that TCF3/E2A is a conserved and specific coregulator of the p21:PUMA expression ratio upon p53 activation acting primarily at the mRNA expression level.

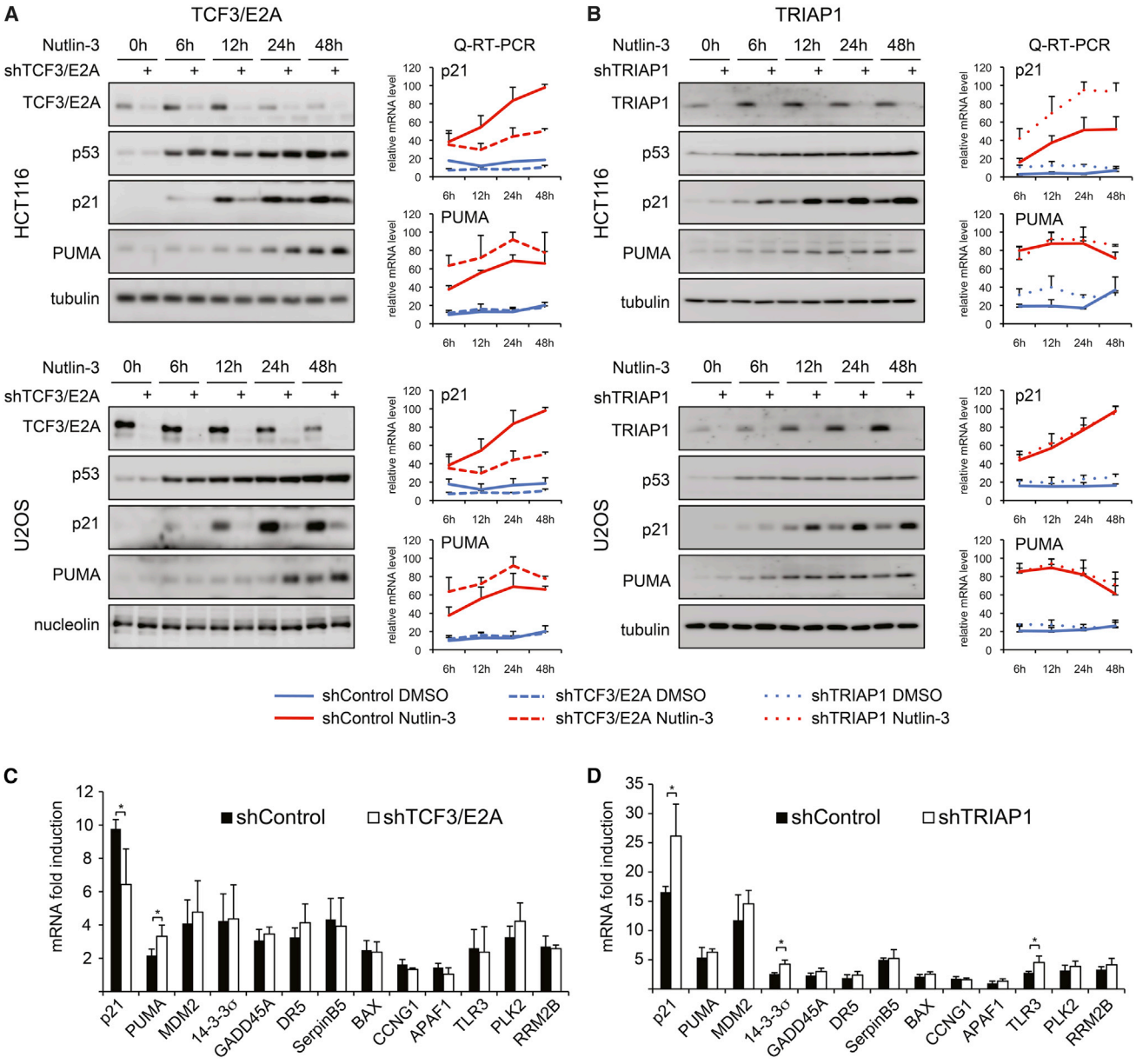

Figure 2. TCF3/E2A and TRIAP1 Control the p21:PUMA Expression Ratio in Diverse Cancer Cell Types

(A) Western blot and qRT-PCR assays show that TCF3/E2A functions as a coactivator of p21 expression and a repressor of PUMA expression in HCT116 colorectal carcinoma cells and U2OS osteosarcoma cells. See Figure S2 for data on A549 lung carcinoma cells.

(B) TRIAP1 functions as a gene-specific repressor of p21.

(C and D) qRT-PCR analysis showing the effects of TCF3/E2A and TRIAP1 knockdown on diverse p53 target genes. All qRT-PCR experiments are expressed as averages of three biological replicates ± SD.

See also Figure S2.

TRIAP1 was previously characterized as a p53 target gene with prosurvival functions (Park and Nakamura, 2005). Indeed, we observed increased TRIAP1 expression upon p53 activation in HCT116, U2OS, and A549 cells (Figures 1E, 2B, and S2B). TRIAP1 was identified in our screen as a factor whose depletion leads to a higher p21:PUMA ratio. In fact, TRIAP1 knockdown increased p21 protein levels in all three cell lines tested throughout the time course of Nutlin-3 treatment (Figures 2B and S2B). In contrast, PUMA expression was not affected by TRIAP1 knockdown. As observed for TCF3, TRIAP1 does not affect p53 accumulation. In HCT116 cells, qRT-PCR analysis demonstrates that TRIAP1 depletion produces an increase in p21 mRNA expression, both basal and induced, with no effects on PUMA mRNA (Figures 2D and S2H). However, this effect on p21 mRNA was not observed in U2OS and is weak in A549 cells (Figures 2B and S2B), suggesting that TRIAP1 may influence p21

protein expression by multiple mechanisms. qRT-PCR analysis of multiple p53 target genes in HCT116 cells showed that TRIAP1 depletion leads to a modest but statistically significant increase in the expression of 14-3-3σ and TLR3 (Figure 2D). Overall, these data indicate that TRIAP1 functions as a p53-inducible repressor of p21 expression across diverse cancer cell types.

TCF3/E2A Does Not Impair p53 Binding or RNAPII Transactivation at the *p21* Locus but Affects p21 mRNA Stability

TCF3/E2A has been previously reported to be a positive regulator of p21 expression (Prabhu et al., 1997), but its mechanism of action has not been elucidated. Chromatin immunoprecipitation (ChIP) analysis of the *p21* locus demonstrates that TCF3/E2A binds to the *p21* locus with peak signals around the transcription start site (Figure 3A). Expectedly, TCF3/E2A binding is much reduced in shTCF3/E2A cells. A modest decrease in TCF3/E2A binding is observed upon Nutlin-3 treatment, which reflects the lower cellular levels of this factor in this condition (Figures 2A and 3A). Importantly, p53 binding to the upstream enhancers in the *p21* locus is not affected by TCF3/E2A knockdown, indicating that TCF3/E2A does not modulate p53 DNA binding activity or chromatin accessibility (Figure 3B). Next, we tested whether TCF3/E2A affects RNA polymerase II (RNAPII) transactivation at the *p21* locus. Toward this end, we performed ChIP assays of total RNAPII, initiating RNAPII (i.e., phosphorylated on serine 5 of the C-terminal domain repeats, S5P) and elongating RNAPII (serine 2 phosphorylated, S2P). In agreement with previous reports (Beckerman et al., 2009; Gomes et al., 2006), we observed that p53 activation leads to increased levels of elongating RNAPII at the *p21* locus, as denoted by higher levels of total RNAPII preferentially in the intragenic region, as well as marked increases in S5P- and S2P-RNAPII at the 5′ and 3′ ends of the gene, respectively (Figures 3C–3E). Interestingly, TCF3/E2A depletion does not affect the basal or induced levels of total, S5P- and S2P-RNAPII, indicating that this factor is not required for p53-dependent transactivation of RNAPII at the p21 locus. Intrigued by this result, we investigated whether the impact of TCF3/E2A depletion on p21 mRNA expression could be explained by effects on mRNA half-life. Indeed, mRNA half-life assays demonstrate that the p21 mRNA is more rapidly degraded in shTCF3/E2A cells, both before and after Nutlin-3 treatment (Figure 3F). This effect is specific, as the half-life of the 14-3-3σ (SFN) mRNA is not affected by TCF3/E2A depletion. Overall, these results indicate that TCF3/E2A does not affect p53 binding or RNAPII initiation or elongation, but acts instead at downstream steps. This could be due to direct action at the *p21* locus to facilitate cotranscriptional RNA processing or indirect action by affecting the expression of posttranscriptional regulators of p21 mRNA stability. Future studies will discriminate among these possibilities.

TCF3/E2A Modulates Cell-Fate Choice upon p53 Activation by DNA Damage in a p21- and PUMA-Dependent Fashion

The ultimate goal of our genetic screen was to identify strategies to manipulate the cellular response to p53 activation via the identification of factors that modulate the p21:PUMA ratio. We found that TRIAP1 represses p21 expression prior to p53 activation (see Figure S2H for RNA data and S3A for protein). Accordingly, we observed decreased levels of bromodeoxyuridine (BrdU) incorporation upon TRIAP1 knockdown in HCT116 and U2OS cells, indicative of slow cell-cycle progression, as well as decreased doubling time of the cell cultures (Figures S3B and S3C). Interestingly, TRIAP1 has been previously characterized as a prosurvival factor (Park and Nakamura, 2005). In agreement with this report, we found that TRIAP1 depletion leads to increased levels of cell death upon DNA damage by doxorubicin (Figure S3D). Thus, although TRIAP1 functions as a repressor of p21, which is often considered an antiapoptotic factor, the overall effects of TRIAP1 on cellular viability cannot be solely explained by its effects on p21 expression.

Next, we focused our efforts on TCF3/E2A. Interestingly, independent previous work from our group identified *TCF3* as a candidate "Synthetic Lethal with Nutlin-3" gene whose knockdown would sensitize cells to Nutlin-3-induced cell death (Sullivan et al., 2012b). In fact, we confirmed that TCF3/E2A depletion increases the apoptotic index upon Nutlin-3 treatment (Figure S3E), which agrees with the observed decrease in the p21:PUMA ratio. In order to further test the impact of TCF3/E2A on cell-fate choice upon p53 activation, we employed doxorubicin, a topoisomerase II inhibitor commonly used in the clinic that induces a DNA damage response leading to a combination of p53/p21-dependent cell-cycle arrest and p53/PUMA-dependent apoptosis (Bunz et al., 1998; Yu et al., 2003). Using an isogenic panel of HCT116 cell lines of varied *p21* and *PUMA* status, we confirmed that *p21* knockout significantly impairs the cell-cycle arrest response upon doxorubicin treatment while sensitizing to apoptosis (Figures 4A and 4B). In this system, *PUMA* knockout has no significant effects on cell-cycle arrest but clearly decreases doxorubicin-induced apoptosis (Figures 4A and 4B). Thus, the cellular response to doxorubicin could be modulated by the p21:PUMA ratio. Importantly, TCF3/E2A depletion in HCT116 cells leads to a significant increase in the number of apoptotic cells upon doxorubicin treatment as measured by Annexin V staining without significant effects on the basal levels of apoptosis (Figures 4C and 4E). This effect is also observed in U2OS cells (Figure S3F). TCF3/E2A knockdown leads to decreased p21 expression, increased PUMA induction and increased levels of active caspase 3 at 24, 48, and 72 hr of doxorubicin treatment without significant effects on p53 accumulation (Figure 4D). Since TCF3/E2A could possibly modulate the expression of hundreds of target genes in the genome beyond *p21* and *PUMA*, we decided to investigate to what extent its effects on cell-fate choice are dependent on these two p53 target genes (Figure 4E). Expectedly, *p21* knockout increases the apoptotic index upon doxorubicin treatment while *PUMA* knockout decreases it (compare y axis values for control shRNA cells). Interestingly, TCF3/E2A knockdown further increases apoptosis in $p21^{-/-}$ and $PUMA^{-/-}$ cells but has no significant effects in the apoptotic index of the double-knockout cells. Thus, we conclude that TCF3/E2A regulates the cell-fate choice upon p53 activation by doxorubicin in a p21/PUMA-dependent manner.

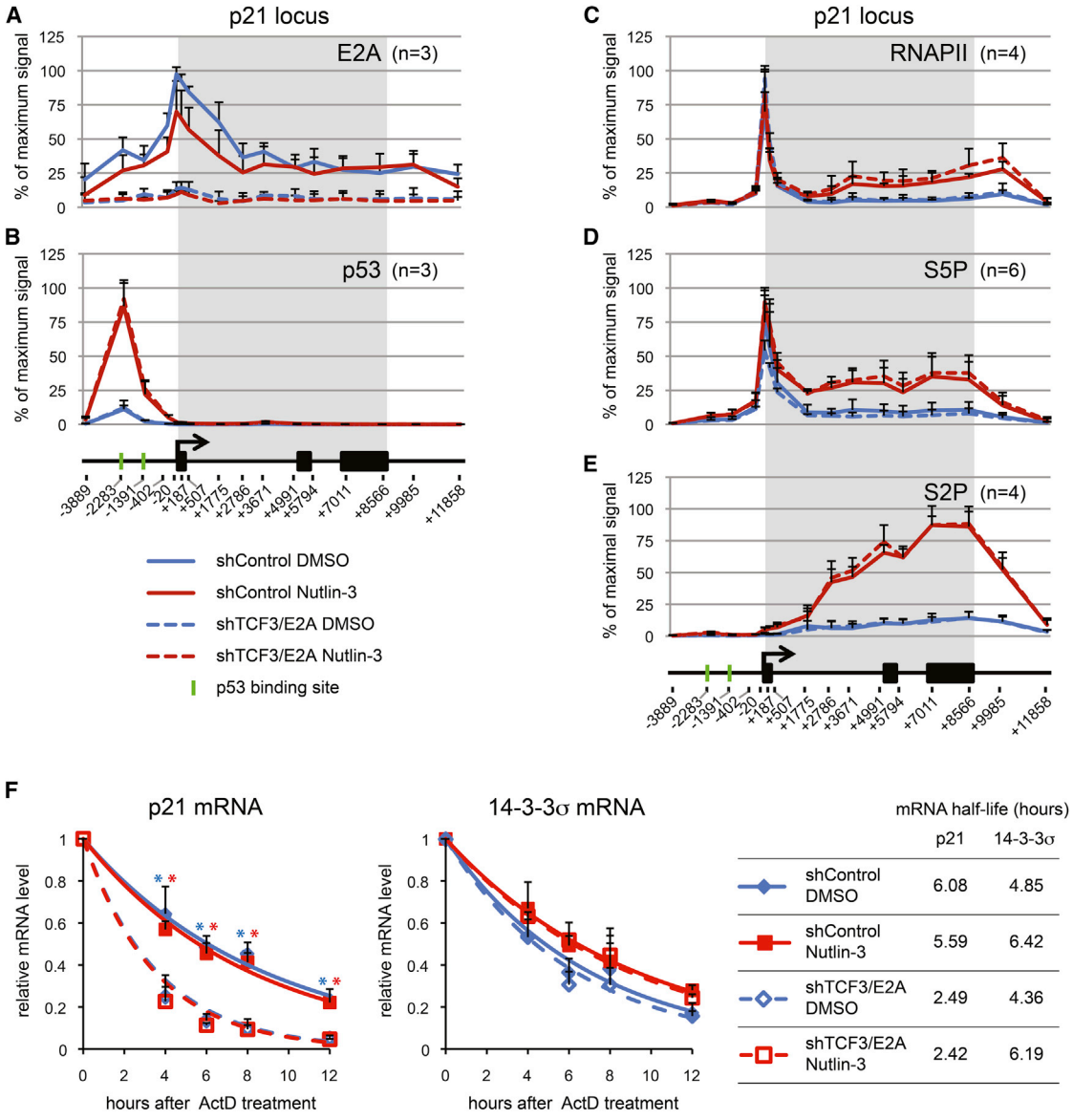

Figure 3. TCF3/E2A Affects p21 mRNA Stability

(A–E) TCF3/E2A binds to the p21 proximal promoter and its depletion does not affect p53 binding or RNAPII transactivation. ChIP analysis of the *p21* locus with antibodies against TCF3/E2A (A), p53 (B), total RNAPII (C), serine 5-phosphorylated RNAPII (S5P, D), and serine 2-phoshoryalted RNAPII (E), in HCT116 cells expressing control shRNA of shRNA against TCF3/E2A, treated with DMSO or 10 μM Nutlin-3 (24 hr). The *p21* gene map is shown at the bottom, with black boxes representing exons and the transcribed region highlighted by a gray box. Numbers at the bottom indicate the position of PCR amplicons used to analyze ChIP-enriched DNA relative to the transcription start site. n indicates the number of ChIPs performed with each antibody.

(F) TCF3/E2A depletion decreases p21 mRNA half-life. mRNA half-life assays were performed for the p21 and 14-3-3σ (SFN) mRNAs by collecting RNA samples at the indicated times after Actinomycin D (ActD) treatment in HCT116 cells expressing control or TCF3/E2A shRNAs, treated with DMSO or 10 μM Nutlin-3 (24 hr). Asterisks indicate significant different ($p < 0.05$) between shControl and shTCF3/E2A samples treated with DMSO (blue) or Nutlin-3 (red) within a given time point. Data are expressed as averages of three experiments ± SD.

DISCUSSION

Pleiotropy is a hallmark of ubiquitously expressed master transcriptional regulators such as p53, NF-kB, and various nuclear hormone receptors, which participate in a plethora of cellular processes by regulating genes involved in distinct functional pathways. Accordingly, the cellular response elicited by activation of these regulators varies greatly with the context, and such pleiotropy often becomes an obstacle to effectively harnessing their activities for therapeutic purposes. In the case of p53, its pleiotropic character limits the therapeutic potential of p53-activating agents. In theory, nongenotoxic MDM2/4 inhibitors could be employed to treat the ~11 million cancer patients currently carrying tumors with wild-type p53, as these agents

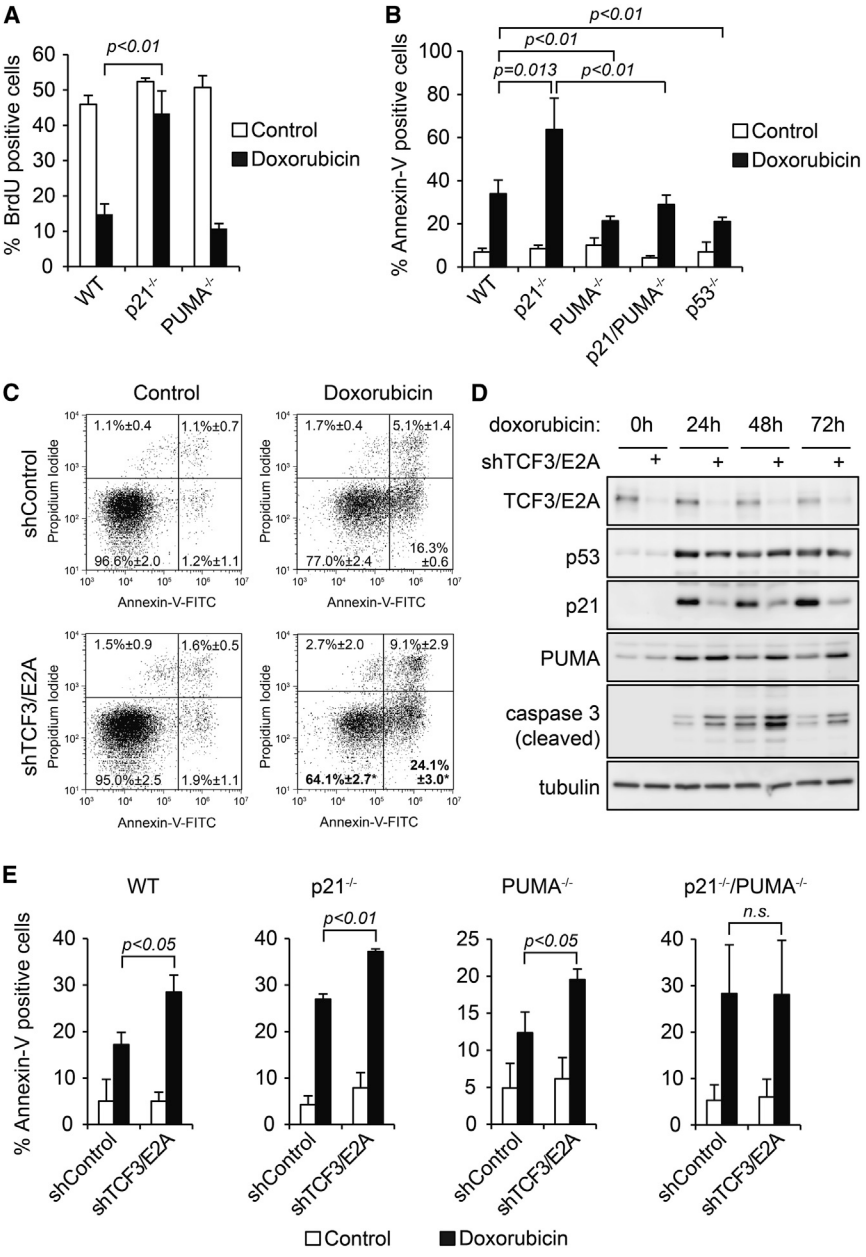

Figure 4. TCF3/E2A Controls the Cellular Response to p53 Activation upon DNA Damage in a p21/PUMA-Dependent Fashion

(A) BrdU incorporation assays demonstrate that p21 is required for the cell-cycle arrest response observed upon doxorubicin treatment (0.5 μM, 12 hr) in HCT116 cells.

(B) Apoptotic index assays show that p21 attenuates p53/PUMA-dependent apoptosis in response to doxorubicin treatment.

(C) TCF3/E2A knockdown increases the apoptotic index of HCT116 cells upon doxorubicin treatment.

(D) Western blot assays show that TCF3/E2A depletion leads to a lower p21:PUMA ratio concurrently with increased levels of activated executioner caspase 3 upon doxorubicin treatment.

(E) TCF3/E2A knockdown enhances the apoptotic index only in cells expressing p21 and/or PUMA. Data in (A), (B), (C), and (E) are expressed as averages of three experiments ± SD. See also Figure S3.

could trigger selective elimination of cancer cells via p53-dependent apoptosis (Brown et al., 2009). However, these compounds trigger p53-dependent apoptosis only in select cancer cell types (París et al., 2008; Tovar et al., 2006). Thus, there is a clear need to identify and characterize the molecular mechanisms defining cell-fate choice in response to p53 activation. Here, we report an experimental approach for the identification of pathway-specific coregulators within a transcriptional program. We employed p53 as the master regulator of choice and its target genes *CDKN1A* (*p21*) and *BBC3* (*PUMA*) as the pathway-specific effectors. Our efforts led to the discovery of many factors modulating the p21:PUMA expression ratio, including TCF3/E2A and TRIAP1.

TCF3/E2A is a member of the class I helix-loop-helix (HLH) transcription factors, or E proteins, not to be confused with *TCF7L1* (also commonly referred to as *TCF3*, a member of the T cell factor/lymphoid enhancer family of transcription factors activated by β-catenin). E proteins are encoded by three genes: *TCF3* (*E2A*), *TCF12* (*HEB*), and *TCF4* (*E2-2*) (de Pooter and Kee, 2010). Additionally, the *TCF3* locus encodes two highly similar splicing variants of E2A, known as E12 and E47, which were first cloned based on their ability to bind an "E-box" sequence in the immunoglobulin K (IgK) light-chain enhancer (Murre et al., 1989). Although E protein transcription factors are ubiquitously expressed, they play unique essential roles in B and T lymphocyte development (de Pooter and Kee, 2010). Mice lacking TCF3/E2A display profound defects in B lymphopoiesis, decreased thymus size, and development of aggressive T cell lymphomas by 3–6 months of age (Engel et al., 2001; Yan et al., 1997; Zhuang et al., 1994). Interestingly, in the absence of TCF/E2A, hematopoietic stem cells (HSCs) and their progeny show increased cell-cycle progression that has been linked to decreased expression of p21 and other CDK inhibitors (Semerad et al., 2009), thus leading to eventual exhaustion of the HSC pool.

Although TCF3/E2A is widely expressed across tissues, its roles outside the immune system are poorly understood. Previous studies have shown that TCF3/E2A binds several E-boxes in the *p21* proximal promoter region and drives p21 expression in HeLa and HEK293T cells with no active p53 (Prabhu et al., 1997). Here, we show that TCF3/E2A is required for full p21

induction upon p53 activation by both nongenotoxic and genotoxic agents in multiple cancer cell types expressing wild-type p53. Thus, p53 and TCF3/E2A act coordinately to enforce p21 expression and cell-cycle arrest in response to p53-activating agents. This effect is exquisitely gene specific, as TCF3/E2A knockdown does not affect induction of many other p53 target genes in diverse pathways. Interestingly, TCF3/E2A seems to act at steps downstream of p53 binding to the *p21* enhancers and RNAPII transactivation at this locus, affecting instead p21 mRNA stability. Strikingly, TCF3/E2A also acts as a gene-specific repressor of PUMA. The *PUMA* locus has an unusual chromatin architecture with constitutive intragenic transcription and internal chromatin boundaries defined by the insulator factor CTCF (Gomes and Espinosa, 2010). We found that TCF3/E2A binds at several sites within the *PUMA* locus (Z.A. and J.M.E., unpublished data). Of note, there is evidence that TCF3/E2A can function as a transcriptional repressor in B cells (Greenbaum et al., 2004). Future studies will focus on elucidating the molecular mechanism by which TCF3/E2A exerts opposite effects on p21 and PUMA expression.

We found that TCF3/E2A depletion leads to increased apoptosis in response to doxorubicin treatment, suggesting that increased expression of TCF3/E2A may protect cancer cells from the killing effects of this commonly used chemotherapeutic agent. Indeed, TCF3/E2A is expressed at high levels in prostate cancer cells where it confers resistance to doxorubicin-induced apoptosis (Patel and Chaudhary, 2012). The *TCF3* locus is a common target of chromosome rearrangements in diverse leukemias leading to E2A chimeric proteins. Interestingly, the chimeric E2A-HLF transcription factor was shown to abrogate p53-induced apoptosis in myeloid leukemia cells by an undefined mechanism (Altura et al., 1998). Our observation that TCF3/E2A is a repressor of PUMA may explain these observations and provide a mechanistic basis for the oncogenic properties of TCF3/E2A chimeras.

Very little is known about TRIAP1, a factor identified in our screen as a specific repressor of p21. Interestingly, TRIAP1 was first characterized as a p53-inducible cell survival factor (Park and Nakamura, 2005). Whereas knockdown of TRIAP1 leads to increased levels of cell death in response to doxorubicin treatment, its overexpression protected against cell death. We confirmed that TRIAP1 functions as a survival factor but also found that TRIAP1 reduces basal p21 protein expression, thus allowing for increased cell-cycle progression as measured by BrdU incorporation (Figures S3A–S3C). We have also confirmed that TRIAP1 is a p53-activated gene as seen by western blot upon Nutlin-3 treatment in multiple cell types (Figures 2B and S2B). Thus, TRIAP1 enables an incoherent feed-forward loop within the p53 network, where p53 induces transcription of both p21 and a p21 repressor. Curiously, whereas TRIAP1 repression of p21 could be explained by effects on p21 mRNA accumulation in HCT116 cells, TRIAP1 seems to regulate p21 levels by other mechanisms in U2OS and A549 cells. Regardless of mechanism, it is clear that the overall effects of TRIAP1 as a prosurvival factor in the p53 network cannot be explained by its function as a p21 repressor, but may be due to other roles. In fact, TRIAP1 was previously found to interact with APAF1 and prevent activation of caspase 9 (Park and Nakamura, 2005). Thus, the inhibitory effect of TRIAP1 on apoptosome activity may override its repressive effect on p21 expression.

In summary, our functional genomics approach has identified several gene-specific regulators within the p53 network, which opens up new research venues not only for defining their mechanism of action, but also for designing strategies for the manipulation of the cellular response to p53 activation.

EXPERIMENTAL PROCEDURES

Cell Culture and Knockdown Cell Line Preparation

HCT116 cells were cultivated in McCoy's medium (Sigma) and U2OS and A549 cells in DMEM (Sigma) supplemented with 10% fetal bovine serum and antibiotic-antimycotic mixture (Life Technologies). Nutlin-3 (Cayman) was solubilized in DMSO and used at 10 μM; doxorubicin (Sigma) was used at 0.5 μM. Individual knockdown cell lines were generated using Sigma Mission shRNA lentiviral plasmids (pLKO.1-puro; see the Extended Experimental Procedures) as described previously (Sullivan et al., 2012b).

Apoptotic Index, BrdU Incorporation, Proliferation, and Cell-Cycle Profile Assays

For apoptosis assays, cells were treated with doxorubicin for 72 hr, and both adherent and floating cells were collected by trypsinization and labeled with Annexin-V-FITC (Invitrogen) and propidium iodide (10 μg/ml) for 15 min in the dark at room temperature and analyzed by flow cytometry (BD Accuri C6, Becton Dickinson). For BrdU incorporation analysis, cells were exposed to doxorubicin for 12 hr. One hour prior to harvest, 1 μg/ml of BrdU was added to the medium, and trypsinized cells were fixed in 70% ethanol. DNA denaturation was performed for 10 min in 2 M HCl with 0.5% Triton X-100 at 37°C. After neutralization with 0.1 M $NaBO_4$, cells were labeled with anti-BrdU antibody and analyzed by flow cytometry. See the Extended Experimental Procedures for antibody information, proliferation assays, and cell-cycle profile analysis. Student's t test was used for statistical analysis.

Western Blotting

Protein samples were subjected to SDS-PAGE and transferred to polyvinylidene fluoride membrane (Millipore). Following incubation in blocking solution and with primary antibody (see the Extended Experimental Procedures for antibody information), HRP-conjugated secondary antibodies and enhanced chemiluminescence solution (Millipore) were used to visualize proteins of interest. Alternatively, for the detection of p21:PUMA ratio, membranes were stained with both antibodies simultaneously. After incubation with fluorescent dye-labeled secondary antibodies, membranes were scanned by Li-Cor system, and band intensities were quantified in Odyssey 3.0.30 software (Li-Cor).

qRT-PCR

Total RNA was extracted using TRIreagent (SIGMA), and template complementary DNA (cDNA) was prepared with the qScript cDNA Synthesis Kit (Quanta Biosciences). cDNA (10 ng) was used per PCR with SYBR Green PCR Master Mix (Applied Biosystems, ABI) and quantified with the Absolute Quantification Method in 7900HT ABI instrument (see the Extended Experimental Procedures for primer information).

See the Extended Experimental Procedures for shRNA screen strategy, ChIP assays, and mRNA half-life assays.

SUPPLEMENTAL INFORMATION

Supplemental Information includes Extended Experimental Procedures, three figures, and three tables and can be found with this article online at http://dx.doi.org/10.1016/j.celrep.2013.04.014.

LICENSING INFORMATION

ACKNOWLEDGMENTS

We are grateful to all members of the Espinosa lab for invaluable discussion and reagents, in particular to Dr. Kelly Sullivan for preparing the HCT116 cells transduced with the shRNA library. This work was supported by NIH grant 5RO1CA117907-07 to J.M.E. and grants from the Cancer League of Colorado and Golfers Against Cancer/AMD Fund to A.C.T. J.M.E. is an HHMI Early Career Scientist. We thank Dr. Luis Fonrouge for inspiration.

Received: December 7, 2012
Revised: March 21, 2013
Accepted: April 17, 2013
Published: May 16, 2013

REFERENCES

Altura, R.A., Inukai, T., Ashmun, R.A., Zambetti, G.P., Roussel, M.F., and Look, A.T. (1998). The chimeric E2A-HLF transcription factor abrogates p53-induced apoptosis in myeloid leukemia cells. Blood *92*, 1397–1405.

Beckerman, R., Donner, A.J., Mattia, M., Peart, M.J., Manley, J.L., Espinosa, J.M., and Prives, C. (2009). A role for Chk1 in blocking transcriptional elongation of p21 RNA during the S-phase checkpoint. Genes Dev. *23*, 1364–1377.

Brown, C.J., Lain, S., Verma, C.S., Fersht, A.R., and Lane, D.P. (2009). Awakening guardian angels: drugging the p53 pathway. Nat. Rev. Cancer *9*, 862–873.

Bunz, F., Dutriaux, A., Lengauer, C., Waldman, T., Zhou, S., Brown, J.P., Sedivy, J.M., Kinzler, K.W., and Vogelstein, B. (1998). Requirement for p53 and p21 to sustain G2 arrest after DNA damage. Science *282*, 1497–1501.

de Pooter, R.F., and Kee, B.L. (2010). E proteins and the regulation of early lymphocyte development. Immunol. Rev. *238*, 93–109.

Echeverri, C.J., Beachy, P.A., Baum, B., Boutros, M., Buchholz, F., Chanda, S.K., Downward, J., Ellenberg, J., Fraser, A.G., Hacohen, N., et al. (2006). Minimizing the risk of reporting false positives in large-scale RNAi screens. Nat. Methods *3*, 777–779.

Engel, I., Johns, C., Bain, G., Rivera, R.R., and Murre, C. (2001). Early thymocyte development is regulated by modulation of E2A protein activity. J. Exp. Med. *194*, 733–745.

Gomes, N.P., and Espinosa, J.M. (2010). Disparate chromatin landscapes and kinetics of inactivation impact differential regulation of p53 target genes. Cell Cycle *9*, 3428–3437.

Gomes, N.P., Bjerke, G., Llorente, B., Szostek, S.A., Emerson, B.M., and Espinosa, J.M. (2006). Gene-specific requirement for P-TEFb activity and RNA polymerase II phosphorylation within the p53 transcriptional program. Genes Dev. *20*, 601–612.

Greenbaum, S., Lazorchak, A.S., and Zhuang, Y. (2004). Differential functions for the transcription factor E2A in positive and negative gene regulation in pre-B lymphocytes. J. Biol. Chem. *279*, 45028–45035.

Henry, R.E., Andrysik, Z., París, R., Galbraith, M.D., and Espinosa, J.M. (2012). A DR4:tBID axis drives the p53 apoptotic response by promoting oligomerization of poised BAX. EMBO J. *31*, 1266–1278.

Kim, J., and Tan, A.C. (2012). BiNGS!SL-seq: a bioinformatics pipeline for the analysis and interpretation of deep sequencing genome-wide synthetic lethal screen. Methods Mol. Biol. *802*, 389–398.

Murre, C., McCaw, P.S., and Baltimore, D. (1989). A new DNA binding and dimerization motif in immunoglobulin enhancer binding, daughterless, MyoD, and myc proteins. Cell *56*, 777–783.

París, R., Henry, R.E., Stephens, S.J., McBryde, M., and Espinosa, J.M. (2008). Multiple p53-independent gene silencing mechanisms define the cellular response to p53 activation. Cell Cycle *7*, 2427–2433.

Park, W.R., and Nakamura, Y. (2005). p53CSV, a novel p53-inducible gene involved in the p53-dependent cell-survival pathway. Cancer Res. *65*, 1197–1206.

Patel, D., and Chaudhary, J. (2012). Increased expression of bHLH transcription factor E2A (TCF3) in prostate cancer promotes proliferation and confers resistance to doxorubicin induced apoptosis. Biochem. Biophys. Res. Commun. *422*, 146–151.

Prabhu, S., Ignatova, A., Park, S.T., and Sun, X.H. (1997). Regulation of the expression of cyclin-dependent kinase inhibitor p21 by E2A and Id proteins. Mol. Cell. Biol. *17*, 5888–5896.

Riley, T., Sontag, E., Chen, P., and Levine, A. (2008). Transcriptional control of human p53-regulated genes. Nat. Rev. Mol. Cell Biol. *9*, 402–412.

Semerad, C.L., Mercer, E.M., Inlay, M.A., Weissman, I.L., and Murre, C. (2009). E2A proteins maintain the hematopoietic stem cell pool and promote the maturation of myelolymphoid and myeloerythroid progenitors. Proc. Natl. Acad. Sci. USA *106*, 1930–1935.

Sullivan, K.D., Gallant-Behm, C.L., Henry, R.E., Fraikin, J.L., and Espinosa, J.M. (2012a). The p53 circuit board. Biochim. Biophys. Acta *1825*, 229–244.

Sullivan, K.D., Padilla-Just, N., Henry, R.E., Porter, C.C., Kim, J., Tentler, J.J., Eckhardt, S.G., Tan, A.C., DeGregori, J., and Espinosa, J.M. (2012b). ATM and MET kinases are synthetic lethal with nongenotoxic activation of p53. Nat. Chem. Biol. *8*, 646–654.

Tovar, C., Rosinski, J., Filipovic, Z., Higgins, B., Kolinsky, K., Hilton, H., Zhao, X., Vu, B.T., Qing, W., Packman, K., et al. (2006). Small-molecule MDM2 antagonists reveal aberrant p53 signaling in cancer: implications for therapy. Proc. Natl. Acad. Sci. USA *103*, 1888–1893.

Vousden, K.H., and Prives, C. (2009). Blinded by the Light: The Growing Complexity of p53. Cell *137*, 413–431.

Yan, W., Young, A.Z., Soares, V.C., Kelley, R., Benezra, R., and Zhuang, Y. (1997). High incidence of T-cell tumors in E2A-null mice and E2A/Id1 double-knockout mice. Mol. Cell. Biol. *17*, 7317–7327.

Yu, J., Wang, Z., Kinzler, K.W., Vogelstein, B., and Zhang, L. (2003). PUMA mediates the apoptotic response to p53 in colorectal cancer cells. Proc. Natl. Acad. Sci. USA *100*, 1931–1936.

Zhuang, Y., Soriano, P., and Weintraub, H. (1994). The helix-loop-helix gene E2A is required for B cell formation. Cell *79*, 875–884.

Cell PRESS
Open ACCESS

EXTENDED EXPERIMENTAL PROCEDURES

shRNA Screen

The HCT116 cell line was transduced with SBI 200K lentiviral library as described previously (Sullivan et al., 2012b). Briefly, HEK293FT cells were transfected with the lentiviral library plasmid DNA and after 48 hr the supernatant containing viral particles was collected and used for transduction of HCT116 cells. Transduced cells were expanded accordingly and treated with 10 μM Nutlin-3 for 48 hr. Following Nutlin-3 treatment, cells were harvested by trypsinization, washed with phosphate buffer (PBS) and fixed with cold 100% methanol for 1 min. The fixation solution was then replaced with 1% bovine serum albumin fraction V (BSA, RPI Corp.) in PBS in three washing steps. $1.5x10^8$ cells were labeled for 4 hr at RT with p21 and PUMA antibodies, washed three times with PBS and incubated for 4 hr with secondary antibodies (see below for antibody information). Median fluorescence intensities (MFI) were calculated subtracting the median intensity value of the sample labeled with an isotype control antibody from the median intensity value of the same sample labeled with either p21 or PUMA antibody. For screening purposes, $3.4 – 4.5x10^6$ cells per population were sorted using LSRII (Becton Dickinson) flow cytometer. Total DNA was extracted using TRIreagent (Sigma-Aldrich) and the shRNA coding loci were PCR-amplified using GNH primers (see below for all primer sequences). Subsequent nested PCR with custom Illumina primers (GNH-ISS) was performed in order to add Illumina-specific sequences. The PCR products were then purified using the QIAquick PCR purification kit (Quiagen). After quantification by NanoDrop (Thermo Scientific), 1.5 pmol of DNA was sequenced on a Genome Analyzer II (Illumina) according to manufacturer's protocol. Sequencing primer (CSP-GNH) and all other primers are listed under *Oligonucleotides* (see below).

In silico analysis of the sequencing data was performed as described previously (Kim and Tan, 2012; Sullivan et al., 2012b). Briefly, image data from the Genome Analyzer II were processed in Illumina software for base identification, quality control and quantification. For screen data analysis we used BiNGS!SL-seq, a bioinformatics pipeline developed for analysis of genome-wide shRNA screens (Kim and Tan, 2012). As a first step, data were pre-processed to exclude poor quality reads. In the second step, sequences were mapped to SBI Reference Library using Bowtie (http://bowtie-bio.sourceforge.net) and a $P \times N$ matrix of read counts (P) and samples (N) was generated. In a filtering step, all sequences mapped to unannotated sequences were removed. The statistical model applied for data analysis was negative binomial. edgeR (http://bioconductor.org/) was used to model the count distribution. To lower the rate of false positive results, we adjusted *p value*s by calculating *q* values of false discovery rate for all shRNAs, where within the group of total samples the median of read counts was higher than the maximum in P1 (or P2) group of samples and vice versa. The post-analysis step involved meta-analysis of adjusted *p* values for all shRNAs associated with one target gene using a weighted Z transformation (Whitlock, 2005), that associates different weights to different shRNAs targeting the same gene (i.e., higher weights on small adjusted *p* values). Using the weighted Z transformation method, we can collapse multiple shRNAs into one *p* value per gene (p(wZ)). This computational method has been successfully applied and validated in recent genome-wide synthetic lethality screens (Casás-Selves et al., 2012; Porter et al., 2012; Sullivan et al., 2012b). Table S1 contains the primary screen data set including shRNA IDs and sequences, target gene IDs, number of shRNAs per gene, read counts in triplicate experiments, adjusted and unadjusted *p* values, log fold change and *p(wZ)* values. All raw input files, the BiNGS code and the output files can be found online at http://tanlab.ucdenver.edu/Joaquin_Zdenek_BiNGS_R211_CellReports.html.

Using a p(wZ) cut-off of 0.01 we selected 81 genes for validation. Selection criteria were as follows: 1) 60 genes overrepresented in either P1 or P2 population based on lowest *p(wZ)* values; 2) Another 20 genes with shRNAs overrepresented in P1 and at the same time underrepresented in P2 population (and vice versa); 3) Five genes were selected based on personal interest of authors. From these total of 85 genes, we could not establish viable stable knockdowns with TRC shRNAs for 4 of them, thus leading to the final list of 81.

Proliferation Assay

HCT116 cells were plated at $2x10^4$ per cm^2 in duplicates. After 24, 48 and 72 hr, cells were harvested by trypsinization, resuspended and counted using Cellometer T4 (Nexcelom Biosciences). Student's t test was used for statistical analysis.

Cell-Cycle Analysis

HCT116 cells were harvested by trypsinization, washed twice with PBS and fixed with 70% ethanol. After fixation, cells were washed twice with PBS/0.1% Triton X-100 and labeled for 1 hr at 37°C using modified Vindelov solution (5 μg/ml of propidium iodide, 33 μg/ml RNase A in PBS with 0.1% Triton X-100). > 16,000 single cells were collected per sample. Acquired data were analyzed using ModFit LT software (Verity Software House).

Chromatin Immunoprecipitation

Chromatin immunoprecipitation was performed as described previously (Gomes et al., 2006). Briefly, HCT116 cells were treated either with DMSO or 10 μM Nutlin-3 for 24 hr. DNA-protein complexes were cross-linked with 1% formaldehyde in PBS for 15 min at room temperature. Formaldehyde was quenched by 0.125 M glycine, and cells were washed twice with ice-cold PBS. Whole-cell lysates were prepared using RIPA buffer (150 mM NaCl, 1% NP-40, 0.5% deoxycholate, 0.1% SDS, 50 mM Tris-HCl pH 8, 5 mM EDTA, 20 μM NaF, 0.2 μM sodium orthovanadate, 5 μM trichostatin A, 5 μM sodium butyrate, and protease inhibitors).

Samples were sonicated and 1 mg of protein extract was pre-cleared with G protein Sepharose beads (GE Healthcare). Supernatants were subjected to overnight incubation with appropriate antibody and G protein Sepharose beads. After multiple washing steps (Gomes et al., 2006) immunocomplexes were recovered, DNA was extracted and used as a template in Q-PCR reaction.

mRNA Half-life Assay

To determine half-life of p21 and 14-3-3σ mRNAs, HCT116 cells were treated with DMSO or 10 μM Nutlin-3 for 8 hr. Following the treatment period cells were exposed to 10 μg/ml Actinomycin D (Sigma-Aldrich) as indicated. Total RNA was extracted and subjected to reverse transcription and qRT-PCR analysis as described in Experimental Procedures. An exponential decay curve was fitted to each set of samples to calculate mRNA half-lives.

Antibodies Used for Flow Cytometry, Western Blots, and Chromatin Immunoprecipitation

For a list of antibodies with manufacturers and catalog numbers used in this study, please see Table S3.

Oligonucleotides

Primers for shRNA library amplification:

F-GNH: TGCATGTCGCTATGTGTTCTGGGA
R-GNH: CTCCCAGGCTCAGATCTGGTCTAA
F-GNH-ISS: CAAGCAGAAGACGGCATACGAAGAAGCAAAAAGCAGAATCGAAGAA
R-GNH-ISS: AATGATACGGCGACCACCGAGATCTACACTCTTTCCCTACACGACGCTTCCTGTCAGA
CSP-GNH: ACACTCTTTCCCTACACGACGCTTCCTGTCAGA

qRT-PCR primer sequences:

p21 Forward: CTGGAGACTCTCAGGGTCGAAA
p21 Reverse: GATTAGGGCTTCCTCTTGGAGAA
PUMA Forward: ACGACCTCAACGCACAGTACG
PUMA Reverse: TCCCATGATGAGATTGTACAGGAC
TCF3/E2A Forward: GCAGCCTAGACACGCAGCCC
TCF3/E2A Reverse: GTAGGCGGTGGCATCCCTGC
14-3-3σ Forward: GCCGAACGCTATGAGGACAT
14-3-3 σ Reverse: CTTCTCCACGGCGCCTT

ChIP Q-PCR primer sequences:

p21 −3889 Forward: CAGCGGCAAGGCCAACAAGC
p21 −3889 Reverse: AGCGCATCAGCCAGTATGAGCC
p21 −2283 Forward: AGCAGGCTGTGGCTCTGATT
p21 −2283 Reverse: CAAAATAGCCACCAGCCTCTTCT
p21 −1391 Forward: CTGTCCTCCCCGAGGTCA
p21 −1391 Reverse: ACATCTCAGGCTGCTCAGAGTCT
p21 −402 Forward: CCTGATCTTTTCAGCTGCATTG
p21 −402 Reverse: GCCCCCTTTCTGGCTCA
p21 −20 Forward: TATATCAGGGCCGCGCTG
p21 −20 Reverse: GGCTCCACAAGGAACTGACTTC
p21 +182 Forward: CGTGTTCGCGGGTGTGT
p21 +182 Reverse: CATTCACCTGCCGCAGAAA
p21 +507 Forward: CCAGGAAGGGCGAGGAAA
p21 +507 Reverse: GGGACCGATCCTAGACGAACTT
p21 +1775 Forward: AGCCGGAGTGGAAGCAGA
p21 +1775 Reverse: AGTGATGAGTCAGTTTCCTGCAAG
p21 +2786 Forward: GCACCATCCTGGACTCAAGTAGT
p21 +2786 Reverse: CGGTTACTTGGGAGGCTGAA
p21 +3671 Forward: CAACTCATGCCTAGCAGAGGGTGG
p21 +3671 Reverse: GGCCAAAGGCCACTGCCCCATA
p21 +4991 Forward: CCAGGGCTGCGATTAGGAA
p21 +4991 Reverse: GTGTCCCTCATGGGTGTGAAT
p21 +5794 Forward: CTGGAGACTCTCAGGGTCGAA
p21 +5794 Reverse: CACATGTCCGCACCTGTCAT

p21 +7011 Forward: CCTGGCTGACTTCTGCTGTCT
p21 +7011 Reverse: CGGCGTTTGGAGTGGTAGA
p21 +8566 Forward: CCTCCCACAATGCTGAATATACAG
p21 +8566 Reverse: AGTCACTAAGAATCATTTATTGAGCACC
p21 +9985 Forward: CACTGCAATTTGGCCCAGA
p21 +9985 Reverse: GTGCAGTAGAGAATTATTCCACATTTG
p21 +11858 Forward: AGGCCTTTTGGGCCCTCGTCT
p21 +11858 Reverse: ATGGCTGACAGTGAGGTGGCA

SUPPLEMENTAL REFERENCES

Casás-Selves, M., Kim, J., Zhang, Z., Helfrich, B.A., Gao, D., Porter, C.C., Scarborough, H.A., Bunn, P.A., Jr., Chan, D.C., Tan, A.C., and DeGregori, J. (2012). Tankyrase and the canonical Wnt pathway protect lung cancer cells from EGFR inhibition. Cancer Res. *72*, 4154–4164.

Porter, C.C., Kim, J., Fosmire, S., Gearheart, C.M., van Linden, A., Baturin, D., Zaberezhnyy, V., Patel, P.R., Gao, D., Tan, A.C., and DeGregori, J. (2012). Integrated genomic analyses identify WEE1 as a critical mediator of cell fate and a novel therapeutic target in acute myeloid leukemia. Leukemia *26*, 1266–1276.

Whitlock, M.C. (2005). Combining probability from independent tests: the weighted Z-method is superior to Fisher's approach. J. Evol. Biol. *18*, 1368–1373.

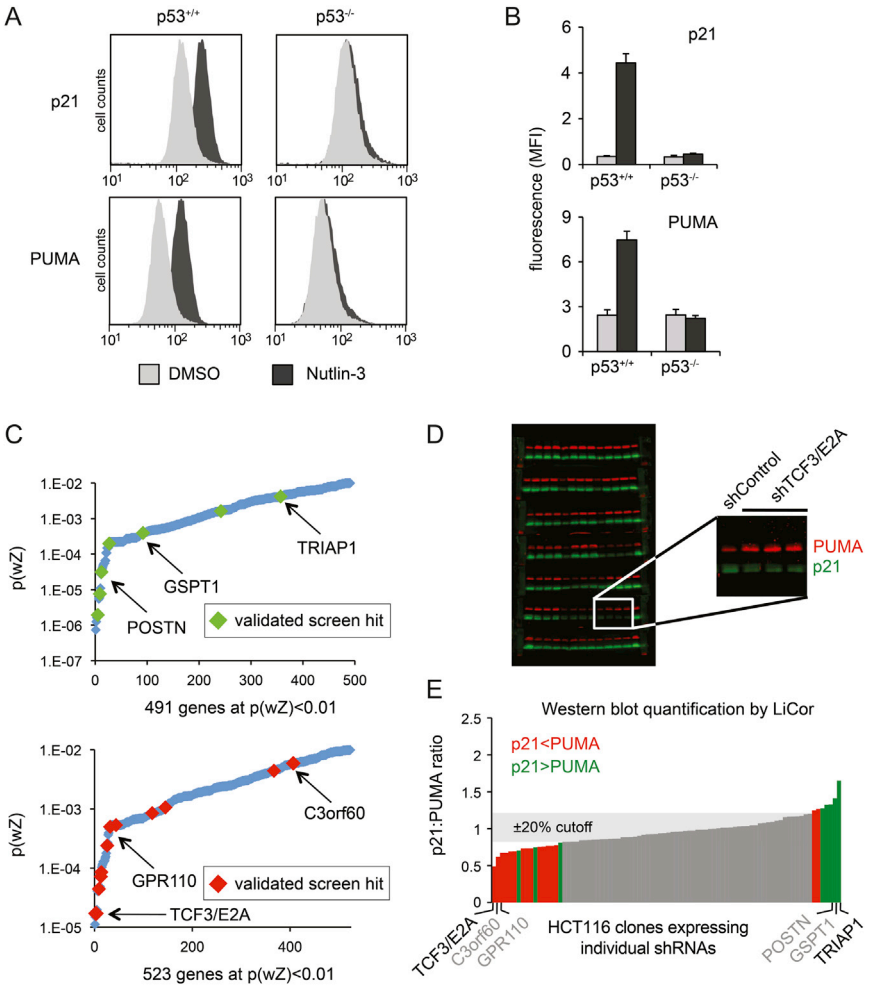

Figure S1. p21 and PUMA Expression Analysis by Flow Cytometry and Screen Results Validation, Related to Figure 1

(A and B) Flow cytometric detection of p21 and PUMA proteins in *p53*$^{+/+}$ and *p53*$^{-/-}$ HCT116 cells. Data are expressed as histograms (A) or median fluorescence intensities (MFI) (B). Data in (B) are expressed as averages of three experiments ± SD.

(C) Histograms displaying screen results as p*(wZ)* values condensing the information of multiple shRNAs against the same gene. Green and red diamonds indicate the position of screen hits validated as in (D).

(D) Validation of candidate genes using independent shRNAs and dual-color Western Blot. p21 and PUMA proteins were detected by two-color multiplexed Western blotting (see the Extended Experimental Procedures for details). HCT116 cells were transduced with shRNAs targeting select candidate genes and treated with Nutlin-3 for 48 hr before preparation of protein extracts.

(E) Quantification of p21:PUMA ratio by Li-Cor, see Table S2 for numerical values.

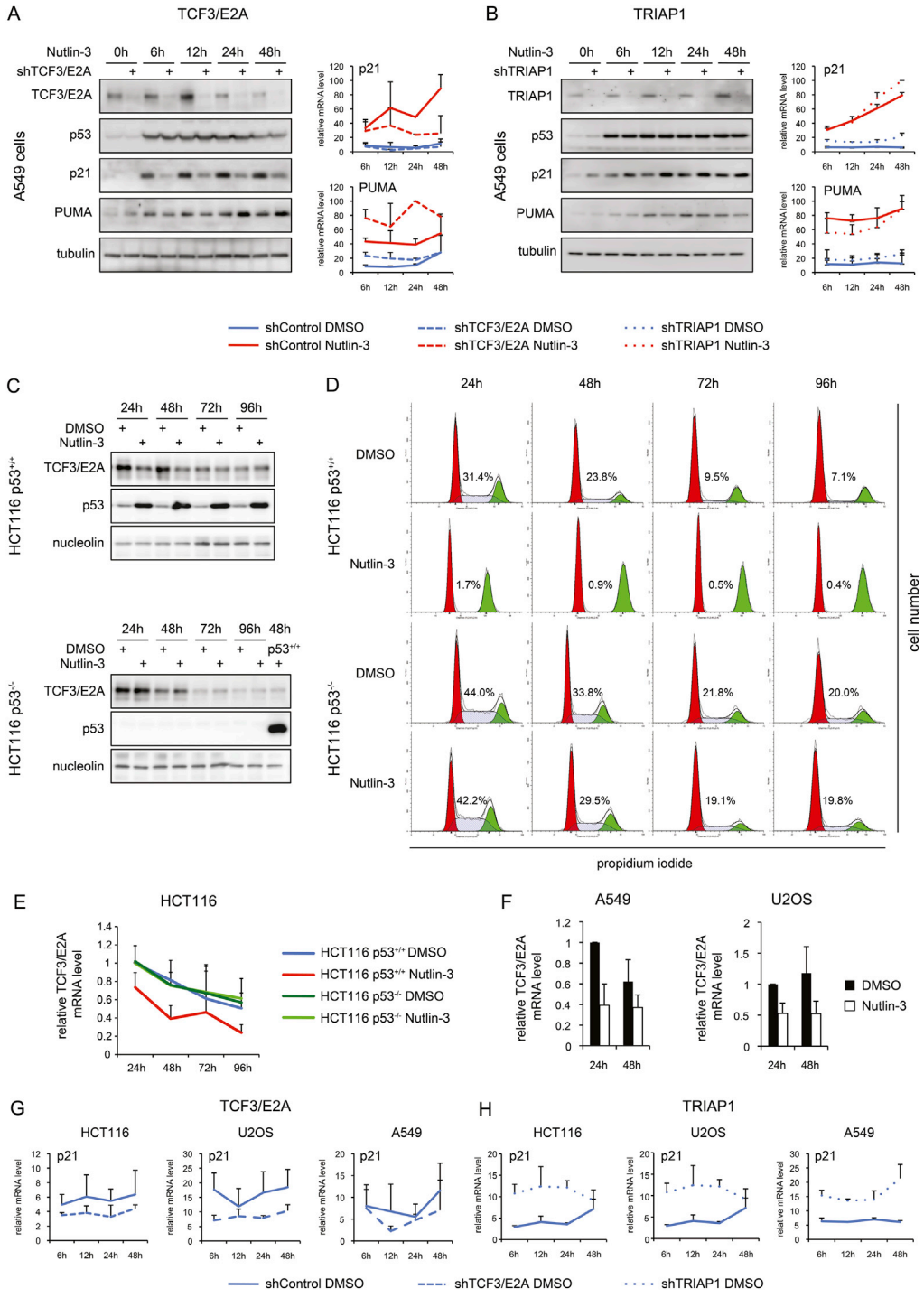

Figure S2. Effect of TCF3/E2A and TRIAP1 Depletion on p21 and PUMA Expression, Related to Figure 2

(A and B) The effects of TCF3 and TRIAP1 are conserved in A549 lung cancer cells. Western blot and qRT-PCR analysis of A549 cells depleted of TCF3/E2A (A) and TRIAP1 (B).

(C) Western blot of TCF3/E2A in HCT116 $p53^{+/+}$ and HCT116 $p53^{-/-}$ cells treated with DMSO or Nutlin-3 as indicated.

(D) Cell cycle analysis of populations treated as in (C). Numbers indicate fraction of cells in S phase.

(E and F) qRT-PCR analysis of TCF3/E2A in HCT116 (E), A549 and U2OS cells (F).

(G and H) qRT-PCR data of DMSO treated samples from Figures 2A, 2B, S2A, and S2B showing the effects of TCF3/E2A and TRIAP1 depletion on basal levels of p21 mRNA expression.

qRT-PCR data are expressed as averages of three experiments ± SD.

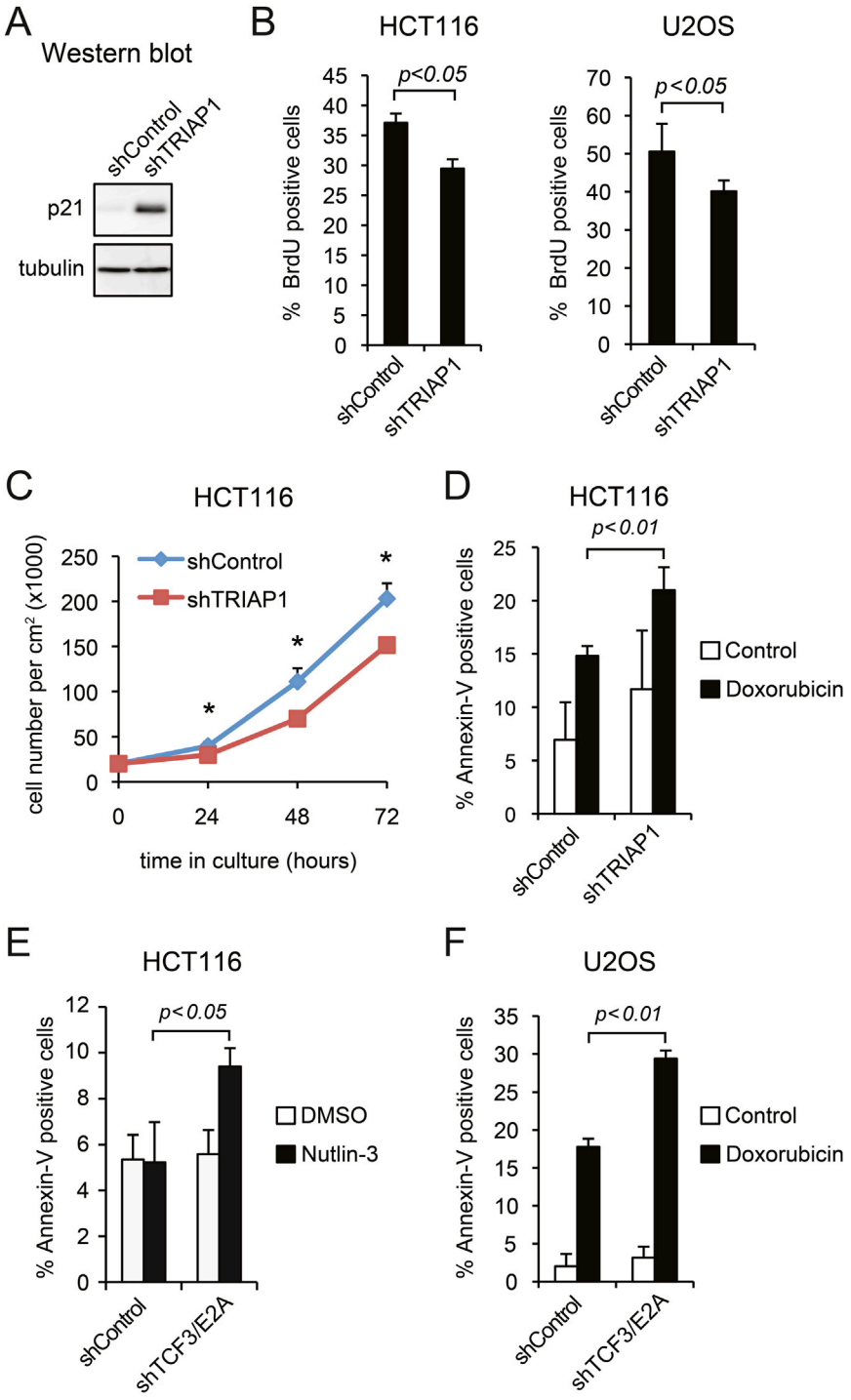

Figure S3. Biological Effects of TRIAP1 Knockdown, Related to Figure 4

(A) Western blot shows increased basal levels of p21 protein in cells depleted of TRIAP1.

(B) Flow cytometric analysis of BrdU incorporation in HCT116 and U2OS cells cultivated for 36 hr.

(C) Cell proliferation assay. Cultivated cells were counted at the indicated times. An asterisk denotes $p < 0.05$.

(D–F) Apoptotic index assays. HCT116 and U2OS cells were exposed to 0.5 μM doxorubicin (D and F) or 10 μM Nutlin-3 (E) for 72 hr, labeled with Annexin-V-FITC and analyzed by flow cytometry.

Data in (B)–(F) are expressed as averages of three experiments ± SD.